FinEstBeaMS - a wide-range Finnish-Estonian Beamline for Materials Science at the 1.5 GeV storage ring at the MAX IV Laboratory

R. Pärna[a,b,*], R. Sankari[b], E. Kukk[c], E. Nõmmiste[a], M. Valden[d], M. Lastusaari[e], K. Kooser[c,a], K. Kokko[c], M. Hirsimäki[d], S. Urpelainen[b], P. Turunen[f], A. Kivimäki[f,b], V. Pankratov[b,f], L. Reisberg[a,b], F. Hennies[b], H. Tarawneh[b], R. Nyholm[b], M. Huttula[f]

[a] *Institute of Physics, University of Tartu, W. Oswaldi 1, EE-51014 Tartu, Estonia*
[b] *MAX IV Laboratory, Lund University, P.O. Box 118, SE-22100 Lund, Sweden*
[c] *Department of Physics and Astronomy, University of Turku, FIN-20014 Turku, Finland*
[d] *Surface Science Laboratory, Optoelectronics Research Centre, Tampere University of Technology, FIN-33101 Tampere, Finland*
[e] *Department of Chemistry, University of Turku, FIN-20014 Turku, Finland*
[f] *Nano and Molecular Systems Research Unit, University of Oulu, P.O. Box 3000, FIN-90014 Oulu, Finland*

Abstract

The FinEstBeaMS beamline is under construction at the 1.5 GeV storage ring of the MAX IV Laboratory at Lund, Sweden. It has been designed to cover an unusually wide energy range from ultraviolet (4.3 eV) to soft X-rays (1000 eV) but experiments will also be possible at the Mg and Al Kα energies. Instead of having two different insertion devices and optical schemes for low and high photon energy regions, we have based our design on a single long-period, elliptically polarizing undulator and a plane grating monochromator. This solution will provide very good conditions for planned experiments in the whole photon energy region. The beamline will have two branches: one will mainly be used to investigate free atoms, molecules and clusters with photoelectron/photoion coincidence spectroscopy as well as solids with photoluminescence spectroscopy whereas the other one will be dedicated to ultra-high vacuum studies of surfaces and interfaces, utilizing X-ray photoelectron spectroscopy and X-ray absorption

*Corresponding author
Email address: rainer.parna@ut.ee (R. Pärna)

spectroscopy. This paper focuses on the optical design of the beamline and general design concepts of the gas phase and solid state end stations.

Keywords: Beamlines, VUV, MAX IV

1. Introduction

The MAX IV Laboratory located at Lund, Sweden is a new synchrotron radiation research centre offering photons for a wide variety of research fields from fundamental physics to biosciences and nanosciences. The facility has constructed two new electron storage rings to offer optimal radiation characteristics in different parts of the electromagnetic spectrum. A 3.0 GeV storage ring provides superior diffraction-limited beam conditions in the soft and hard X-ray regions. A 1.5 GeV ring will offer excellent beam quality in the energy range from ultraviolet radiation to soft X-rays. This smaller storage ring is currently under commissioning. Finland and Estonia have agreed to construct in collaboration a beamline at the 1.5 GeV ring; it is one of the fourteen beamlines financed so far at the MAX IV Laboratory.

FinEstBeaMS (Finnish - Estonian Beamline for Materials Science) is a materials science beamline at the 1.5 GeV storage ring of the MAX IV Laboratory. It has two branch lines: one for research of free atoms, molecules and clusters and the other for ultra-high vacuum (UHV) surface science studies but it will also be possible to attach user setups to end stations. Investigations will range from electronic structure studies of atoms, molecules and clusters in gas and vapor phase to formation analysis and nanoscale characterization of surfaces.

The beamline will cover a wide photon energy range, 4.3 - 1000 eV, and give an opportunity to probe core and valence levels with a focused or defocused beam using light, produced by an elliptically polarizing undulator (EPU), with variable polarization. Two insertion devices would have allowed one to design optimized light sources for both low and high photon energy regions, which solution has been adopted, for example, at the Pleiades beamline at Soleil [1]. However, here the starting point was a single insertion device that will utilize

the whole straight section length of 2.5 m. A plane grating monochromator illuminated with collimated light (cPGM) [2] will select photon energies for experiments. It can operate at low photon energies when equipped with a very sparsely ruled grating. Some beamlines have solved operation in extended photon energy ranges by combining normal incidence monochromators (NIM) and grazing incidence monochromators [3, 4]. Light diffracted into higher orders at low energies is a common problem in grazing incidence monochromators, but the issue can be solved by a combination of gas and thin-film filters. After the monochromator, the light will be directed to the selected branch line by using one of the two toroidal focusing mirrors. This solution does not require a separate switching mirror, thus reducing reflection losses. The spot size in focus at both branch lines will be 100 μm $\times$ 100 μm (about 200 μm $\times$ 100 μm in the wiggler mode, values are given as horizontal size $\times$ vertical size). This is suitable for most spectroscopy experiments and will be achieved by using demagnifying ellipsoidal refocusing mirrors.

In the following we describe the undulator source and the optical design of the beamline, estimate power loads on the optics, photon energy resolution, photon flux and spot size at experiment as well as give a short overview of the experimental end stations.

2. Source

The photon source of the beamline will be an EPU. It has 25 full periods of 95.2 mm and half a period at each end, resulting in a total magnetic structure length of 2475.2 mm. The device is based on the APPLE II design [5]. **It has been built at the MAX IV Laboratory using a novel technique developed in-house and based on gluing pairs of permanent magnets [6]**. All four arrays of magnets can be shifted in the longitudinal direction which allows full control of the light polarization. As estimated by using the SPECTRA program [7], the total maximum power of the insertion device will be 2.4 kW, of which at most 650 W will be accepted by the beamline. **Table 1**

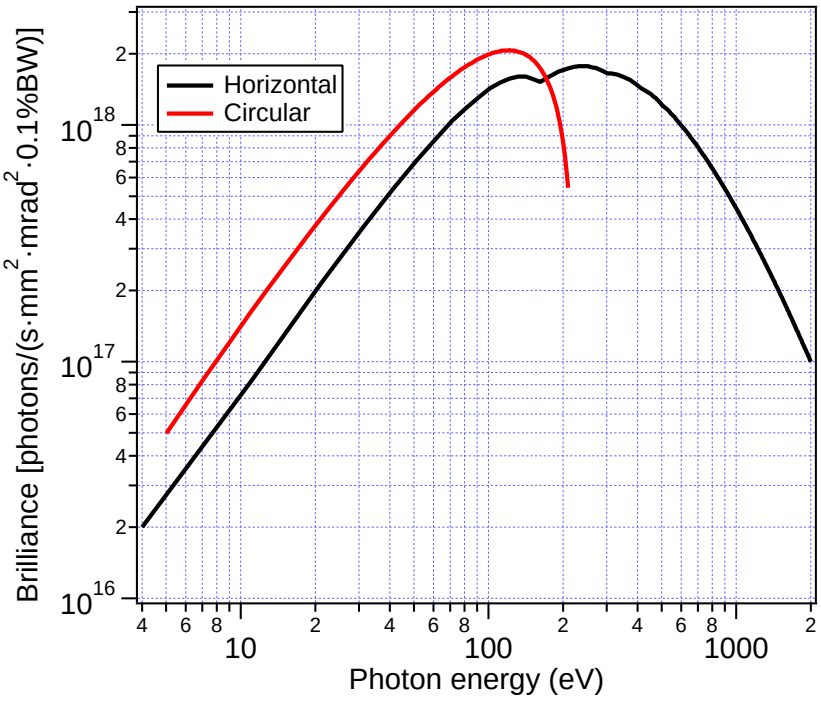

Figure 1: **The estimated brilliance of the elliptically polarizing undulator for the horizontal and circular modes using the minimum gap and 500 mA beam current.**

summarizes the parameters of the undulator in different modes of operation. The undulator will be installed in the 1.5 GeV electron storage ring during the summer shutdown in 2017.

The first undulator harmonic will cover in the circularly polarized mode the photon energy range of 4.9-207 eV. The degree of circular polarization will then be almost 100%. It will typically go down to 70-80% at higher photon energies where higher harmonics have to be used. From 11 eV onwards, the state of polarization can completely be controlled up to about 200 eV, i.e., any beamline induced changes in polarization can be fully compensated in this photon energy range. **The brilliance of the EPU in the horizontal and circular polarization mode is shown in Fig. 1. The brilliance in the vertical mode is similar to that in the horizontal mode except that**

Table 1: **Summary of the parameters of the elliptically polarizing undulator in different modes of operation. hν_{min} is the minimum achievable photon energy. Total radiated power has been calculated with 500 mA ring current.**

Polarization	Effective K	hν_{min} (eV)	Total power (kW)
Horizontal	K_y=10.40, K_x=0.00	4.1	2.4
Vertical	K_y=0.00, K_x=8.71	5.7	1.7
Circular	K_y=K_x=6.67	4.9	2.0
Inclined 45°	K_y= K_x=4.70	9.6	0.9

the curve begins at a higher photon energy.

For a medium energy storage ring such as the MAX IV 1.5 GeV ring, the deflection parameter K of an undulator must be relatively high to reach low photon energies. For the present undulator the effecitive K=10.40 when the gap will be closed to its minimum value, 14 mm. Then the high photon energy part of the undulator spectrum will resemble that of a wiggler. Furthermore, running the undulator as a wiggler will provide quite high photon flux at high photon energies: at 1000 eV the estimated flux at the sample still exceeds 10^{12} photons/s at 0.1% bandwidth. This means that experiments will also be feasible at 1253 eV and 1486 eV, allowing direct comparison to results obtained with Mg and Al Kα X-ray sources.

3. Optical Design

The optical layout of the FinEstBeaMS beamline is shown in Fig. 2. The beam height at the center of the undulator will be 1300 mm. The first optical element in the beamline will be a side-cooled toroidal mirror (M1) situated 12 m from the source. It will collimate the beam both vertically and horizontally. The monochromator **is of SX700 type and it was manusfactured by FMB, Berlin.** It consists of an internally cooled plane mirror (M2) and two side-cooled plane gratings (PG1, 600 l/mm and PG2, 92 l/mm). Steep angles at a grating are required to reach low photon energies with a grazing incidence monochromator, even when the ruling density is low. At the same time, gratings

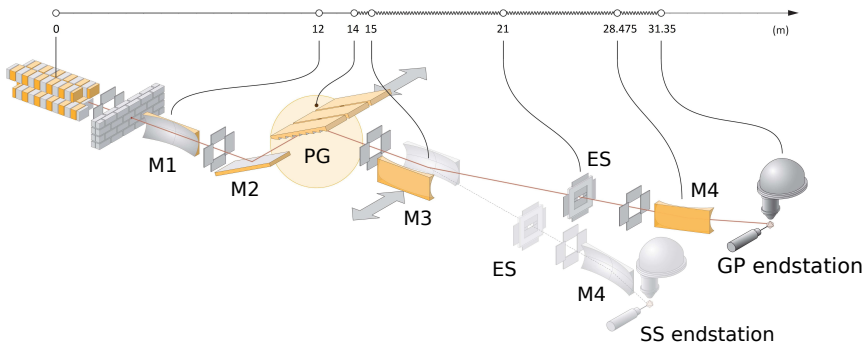

Figure 2: The optical layout of the FinEstBeaMS beamline is based on the plane grating monochromator illuminated with collimated light. A toroidal mirror M1 will collimate the incident synchrotron beam in both directions. Toroidal focusing mirrors M3 will focus wavelength-dispersed radiation from the plane grating to the exit slits and also act as switching mirrors, directing the radiation to either of the two branch lines. Ellipsoidal refocusing mirrors M4 will focus monochromatic radiation both vertically and horizontally at the experiments. The following abbreviations are used: M1–M4 = mirrors, PG = plane grating, ES = exit slit, GP = gas phase, and SS = solid state.

need to be considerably long to collect all radiation from the source also at higher energies. These requirements result in a relatively high offset of 32 mm between the incoming and outgoing radiation. The dispersed radiation from the grating will be focused by an uncooled toroidal focusing mirror, $M3_{GP}$ or $M3_{SS}$, at the exit slit in the gas phase branch or in the solid state branch. The exit slits will be located 6 m away from the focusing mirrors. The light will be switched between the branch lines by inserting either of the two focusing mirrors into the beam path. No separate switching mirror is needed in this optical scheme.

A single ellipsoidal mirror ($M4_{GP}$ or $M4_{SS}$) will refocus monochromatized radiation in each branch. It will deflect the beam sideways, keeping it in the horizontal plane. The beam height will be 1332 mm at the experiment. For the best photon energy resolution it is beneficial to have both the horizontal and vertical intermediate focuses at the exit slit plane. In the present case the demagnification towards the exit slit will be modest ($\times 2$) and a further demagnification of 2.6 will still be needed to produce a 100 μm horizontal spot

size at the sample plane. To increase the separation between the end stations at the two branch lines, the entrance and exit arms of the refocusing mirror in the gas phase branch line have been set at 7.475 m and 2.875 m, respectively, while they are 6.500 m and 2.500 m, respectively, in the solid state branch line. As an additional asset, the use of a single ellipsoidal mirror for refocusing demagnifies the exit slit vertically by a factor of 2.6. Relatively large exit slit values can therefore be used to increase photon flux while the vertical beam size at the sample will still remain below 100 μm. A toroidal refocusing mirror cannot be used here even though demagnification is modest: at low energies the source will be strongly divergent and collection of all radiation would result in a large, coma-dominated image at the focal plane. Also the ellipsoidal mirrors suffer from aberration when imaging extended, diverging sources but images at the focal plane remain acceptable even at low photon energies (see Section 4.4).

The exit slit is adjustable, extremely accurate and acts in the dispersion plane. If necessary, the horizontal beam size can be reduced with horizontal baffles that are located in the same unit as the exit slit. The use of the baffles will naturally reduce photon flux. As the refocusing mirror will directly image (and demagnify) the beam size at the horizontal baffles into the plane of experiments, baffling will result in a decreased image size. It would have been possible to tailor refocusing to obtain optimal spot sizes for various experiments but refocusing with a single ellipsoidal mirror is a very simple solution, meets the requirements, and allows us to reach high photon energies with good efficiency. Basic information about all the optical components and distances between them in the beamline is given in Table 2.

4. Expected performance

4.1. Power load

An undulator with a large K value is required in order to reach low photon energies at the 1.5 GeV storage ring. This means in practice both strong magnets (B_{max}=1.13 T) and a large period length. Such devices produce high power

Table 2: Parameters of the optical elements. All mirrors except for M1 have already been delivered. Slope errors are given in the form (*tangential slope error/sagittal slope error*).

Optical element	M1	M2	$M3_{GP}$	$M3_{SS}$	exit slit	$M4_{GP}$	$M4_{SS}$
Shape	toroid	plane[1]	toroid	toroid	rectangle	ellipsoidal	ellipsoidal
Deflection	hor.	vert.	hor.	hor.	-	hor.	hor.
Distance (mm)	12000	var.	15000	15000	21000	28475	27500
Incidence angle	2°	0°-20°	2°	2°	-	2°	2°
Geom. size (mm)	520×40×60	560×60×60	420×60×60	420×60×60	-	430×60×60	380×60×60
Opt. size (mm)	500×20	490×20	400×40	400×40	adj.	414×46	360×40
Substrate material	Si	Si	Si	Si	-	Zerodur	Zerodur
Coating	Au 866 Å	Au 400 Å/ Pt 80 Å	Au 679 Å	Au 636 Å	-	Au 400 Å	Au 400 Å
Roughness (Å)	2.8	1.1	1.6	2.0	-	1.7	2.0
Slope error (arcsec)	0.21/0.68	0.066/0.037	0.12/0.44	0.11/0.47	-	0.68/2.46	0.37/0.48
Entrance arm (mm)	12000	-	∞	∞	-	7475	6500
Exit arm (mm)	∞	-	6000	6000	-	2875	2500
Parameters	R=691.1 m	R=123.5 km	R=343.9 m	R=344.4 m	width	a=5175 mm	a=4500 mm
		r=31.9 km			0...4 mm	b=161.8 mm	b=140.7 mm
	ρ=836.2 mm		ρ=420.2 mm	ρ=420.2 mm	height	y_0=144.9 mm	y_0=126.0 mm
					0...500 μm	z_0=-2301 mm	z_0=-2001 mm
						ϕ=0.889°	ϕ=0.889°

[a]Plane means that the radii along, and perpendicular to the length are larger than 50 km and 10 km, respectively.

because total power is proportional to the square of K. The present undulator will produce 2.3 kW when tuned to the minimum energy of 4.3 eV. Although the total power of an undulator with a high K value is in general higher than that of an undulator with a low K value, the power densities of equally long devices do not scale similarly. As an example, we can compare the present undulator, with $K = 10.065$ at 4.3 eV, to the undulator of the SPECIES beamline [9] at the MAX IV Laboratory. That undulator was designed for an equally long straight section and to have $K_{max} = 4.88$ at 27 eV. When tuned to produce the lowest photon energies of 4.3 and 27 eV at the FinEstBeaMS and SPECIES beamlines with the fundamental harmonic, their undulators are calculated to have on-axis power densities of 810 W/mrad^2 and 930 W/mrad^2, respectively. As the higher power density causes larger deformations on optical elements, the present undulator will not actually set extreme demands for cooling of the optical elements. The total power into the beamline acceptance, about 600 W, will actuallly be less than to which soft X-ray beamlines at the already decommissioned MAX II storage ring were exposed. The beamline acceptance has been chosen to be relatively large, 1.5 mrad $\times$ 1.3 mrad (hor.$\times$vert.) to have as smooth a heat bump profile as possible.

The heat load deformations were deduced from power calculations performed with SRCalc [10] and the following finite element analysis (FEA) method in COMSOL Multiphysics [11]. According to earlier experience with the SPECIES beamline, side cooling will be sufficient for M1 and the gratings, but M2 should be an internally cooled mirror. A relatively large grazing incidence angle on M2, 20° in maximum, can otherwise result in unacceptable deformations. Deformed surfaces were inserted in RAY [12], a ray tracing program developed at BESSY. The deformations were not found to deteriorate the beamline performance.

4.2. Photon energy resolution and flux

Different contributions to the resolving power can readily be calculated for a cPGM monochromator [2]. One can roughly decompose resolution defining terms into four categories: source size, slope errors of the optics, slit size and the

diffraction limit set by the grating illumination. The three first contributions are usually implemented into ray tracing programs whereas the diffraction limit is added separately assuming that quadratic summing is adequate. We took the diffraction limit into account analytically by calculating the number of grating lines illuminated by the coherent core of the undulator radiation (2σ') and multiplying the result by 1.13 (see Ref. [13] for motivation). The diffraction limit was checked in simulations by placing a diffracting aperture before the grating. The vertical size of that aperture was set to correspond to the opening angle of the coherent core of the undulator radiation.

The electron beam size and divergence were convoluted with the diffraction-limited size and divergence to obtain the source size in the undulator mode. At low emittance storage rings, like those at the MAX IV Laboratory, the actual source size (σ) and divergence (σ') are dominated by the diffraction limit and its absolute contribution becomes an important question. For these simulations we adopted the approximate equations presented by Elleaume [14]:

$$\sigma' = \sqrt{\frac{\lambda}{2L}} \; and \; \sigma = \frac{\sqrt{2\lambda L}}{2\pi}, \tag{1}$$

where L is the undulator length and λ is the emitted wavelength. Compared to the commonly used Gaussian beam approximation, the source size is about double when on-axis energies are observed.

As mentioned above, photon flux from the present insertion device at high photon energies will actually be higher when the device is used as a wiggler rather than as an undulator with some high harmonic tuned to the same high photon energies. In the pure wiggler approximation [15] both the source size and divergence are, however, very different from those in the undulator approximation. We performed therefore more rigorous source calculations for the wiggler mode. The electron orbit in the insertion device was first obtained by RADIA [16], whereby a magnetic model with realistic magnet properties was used for the whole device. This orbit was used as an input for SPECTRA [7], in which near-field calculations were used to observe the radiation pattern 10 m away, showing the divergence. It is also possible to see the spatial extent of

the source in the same program. For example at 1000 eV, the source is close to a Gaussian with 460 μm $\times$ 120 μm (FWHM) (hor. x vert.). The horizontal divergence resembles a hard edge with an opening of 8 mrad, whereas the vertical divergence is well presented by a Gaussian with 0.54 mrad width (FWHM). The divergence agrees well with the values given by the wiggler approximation [15], whereas the rigorous calculations show that the expected vertical source size is about 50% larger and the horizontal source size 50% smaller than the approximations predict. Nevertheless, both the size and divergence of the source will be much larger when using the insertion device as a wiggler rather than as an undulator. The wiggler mode will provide more flux at high energies: the gain will be about 2.5 at 1000 eV and even larger at still higher energies. However, the horizontal spot size at the sample plane will also become larger, about 200 μm.

Two blazed gratings will be used to cover the wide energy range with good photon energy resolution. The low density grating will work at very low energies, below some tens of eVs, whereas the medium density grating was designed to cover the energy range from 17 eV to 1000 eV, but it will actually be usable up to about 1500 eV.

In a cPGM, focusing the beam by some means close to the exit slit has been found to increase the resolving power both in initial simulations performed for the FinEstBeaMS beamline and in practice [18]. The cPGM requires a collimating mirror (M1) before and a focusing mirror (M3) after the monochromator. Strocov *et al* [19] showed that the beam should be focused horizontally by the collimating mirror, not by the focusing mirror, in order to obtain higher energy resolution. The original cPGM scheme [20] is nevertheless used in the present beamline: M1 will collimate the beam both vertically and horizontally, while M3 will focus radiation at the exit slit both horizontally and vertically. Higher demagnification of the horizontal source size at the exit slit is an advantage of this scheme. At this beamline, a small decrease in the resolving power will actually be **more acceptable than an increase of the spot size by more than 30%. For example, at 150 eV photon energy, the practical res-**

olution limit with the chosen configuration is calculated to be about 11.4 meV and the image at the sample plane will be about 90 μm wide. If M1 were a cylindrical mirror, the respective values would be 10.5 meV and 130 μm.

The FinEstBeaMS beamline was modeled with the program RAY [12]. The size and quality of the optical elements were as given in Table 2. The deformation of the optics described above was included as a vertical displacement on the surfaces of the first two mirrors and grating(s). We first tested the resolution predicted by the analytical model by ray tracing. The correspondence was excellent and showed that the resolution is mostly limited by **the source size, which is enlarged by the diffraction limit, when the monochromator is used in a low angular magnification mode. Here the low angular magnification mode is taken to cover the values of** $c = cos\beta/cos\alpha \leq \mathbf{6}$, where α and β are the incidence and diffraction angles of the grating, respectively. With higher values of c the contribution of the source size to photon resolution reduces and slope errors, mostly those of the gratings, become dominant. However, the required resolving power, R=5000-10000, can be achieved in the whole photon energy range. **We estimate that the beamline has a sub-meV resolution up to 40 eV and 20-30 meV resolution at the carbon 1s edge (h$\nu \sim 290$ eV). The chosen monochromator allows one to switch easily between high-resolution and high-flux modes but high resolution comes with reduced photon flux.**

A standard way to compare beamlines is to show photon flux at a certain resolving power over the photon energy range of the beamline. Figure 3 shows the result of simulations for R=5000, a typical setting foreseen in most experiments.

4.3. Higher order suppression

The use of a low line density grating at low energies means that incidence angles on both the plane mirror and the grating in the monochromator will be much closer to grazing incidence angles than in any NIM monochromators. Combined with the grazing incidence mirrors of the beamline, this configuration

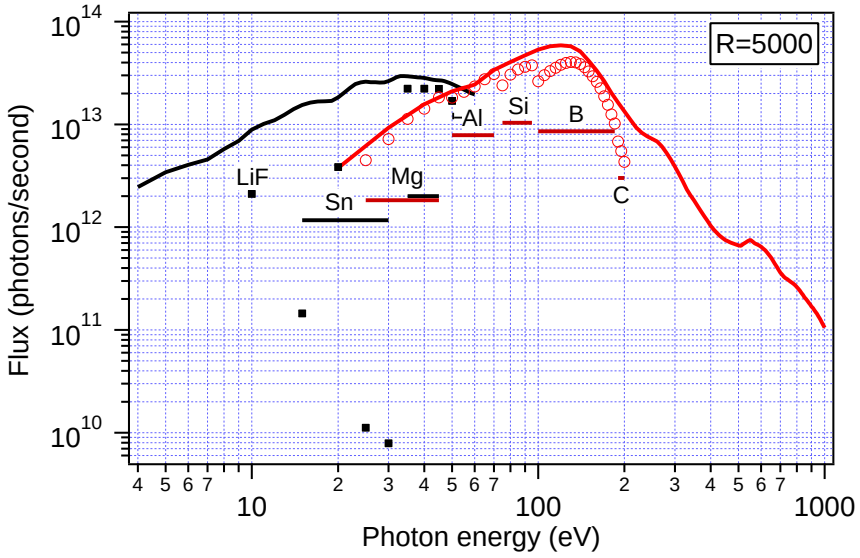

Figure 3: Estimated photon flux at experiment for the 92 l/mm grating (curve at left, black colour) and the 600 l/mm grating (curve at right, red colour) for resolving power of 5000, i.e. 0.02% band width. Beamline acceptance was set at 1 mrad×0.2 mrad, and it was assumed that the most efficient undulator harmonic is tuned for each photon energy. **A ring current of 500 mA was used in these calculations. Solid squares and open circles show the first order flux for the two gratings after using filters of 200 nm thickness under the condition that the sum of the second and third order flux is 1% or less of the first order flux. Horizontal bars depict the energy ranges of the different filters.**

will be prone to poor high order suppression. A set of tools has been chosen to overcome this problem. Up to 11.8 eV, a LiF filter can be used. At higher energies Sn ($4d$ BE 23.9 eV), Mg ($2p$ BE 49.6 eV), Al ($2p$ BE 72.5 eV), Si ($2p$ BE 99.2 eV), B ($1s$ BE 188 eV) and C ($1s$ BE 284.2 eV) filters can be used to cover almost the whole operation range of the first undulator harmonic. However, in the region approximately between 25 and 50 eV, Mg $3s$ absorption also reduces the first order efficiency by 20-40% [8]. Transmission increases relatively fast after the $1s$ absorption edges of boron and carbon, but undulator radiation will be more condensed into the first harmonic at those energies, helping to reduce the high order contamination. It is also possible to use noble gas absorption as high order filter, which solution has been adopted at the BLOCH beamline at MAX IV.

The effects of the filters on higher order suppression were estimated as follows. Using the RAY package and the value of $c = 2.25$, we calculated the photon flux in the first, second and third order at 5 eV intervals in the energy range of the first undulator harmonic. The calculations covered the energy range of 5-50 eV for the 92 l/mm grating and of 25-200 eV for the 600 l/mm grating. These fluxes were then multiplied by the transmission of the selected filters (all had the thickness of 200 nm). The first order flux corresponding to the situation where the sum of the second and third order light was 1% or less of the first order flux is reported in Fig. 3. At each point a filter fulfilling the 1% criterion has been chosen. The use of the Mg filter with the 92 l/mm grating at the photon energies of 25 and 30 eV does not fullfil this condition: the contribution of higher orders would be about 7% and 4% at these energies, respectively, where the first order flux is calculated to be $\sim 2 \cdot 10^{13}$ photons/s. The same filter with the 600 l/mm grating will give much better higher order suppression. The difference is due to the fact that the incidence angle is much larger with the 600 l/mm grating (e.g., 11.2° at 25 eV) than with the 92 l/mm grating (4.4° at 25 eV). We therefore conclude that it will

be better to use the 600 l/mm grating from about 20 eV upwards.

4.4. Refocusing optics and spot size

The requirement of good energy resolution dictates the beamline design from the beginning. The intermediate horizontal focus at the exit slit plane is a demagnified image of the horizontally large source. With present distances the horizontal image size at the exit slit will be exactly half of the source size, amounting to 320–220 μm in the photon energy range of the beamline. At low energies the diffraction limit enlarges the apparent source and the horizontal size of the image at the experimental plane is slightly larger than 100 μm up to about 20 eV. As the beamline is aimed to work up to 1000 eV photon energy, the number of mirrors should be kept as low as possible to avoid not only reflection losses but also expensive and often complicated optical schemes.

A stigmatic focus at the exit slit and a relatively modest need for demagnification provide good conditions for refocusing. Demagnification was chosen to be 2.6 for both the branch lines. Experience has shown [15] that spherical surfaces (spheres, toroids) can be used up to demagnification of 10 without severe aberrations but that argument is not valid here: The divergence of the photon beam at low photon energies is large, resulting in a long illuminated area on the mirrors. This in turn gives rise to very strong aberrations, mostly coma, and the image becomes unacceptable. Although images formed by any single optical element working in grazing incidence angles suffer from coma [21], an ellipsoidal mirror has best imaging capabilities. For example, imaging a highly asymmetric object, the exit slit, will result in a well-known bow-tie shape of the image. This effect also depends on the beam divergence and on the acceptance angle of the mirror, meaning that it is largest at low photon energies and with high demagnification of the monochromator. On the other hand, the stigmatic focus at the exit slit, which is a prerequisite for the use of an ellipsoidal mirror, means that the source of the ellipsoidal mirror becomes more symmetric. Actually, the highest reduction of the horizontal beam size at the exit slit would have been obtained by having a diverging beam until the toroidal mirror M3, but

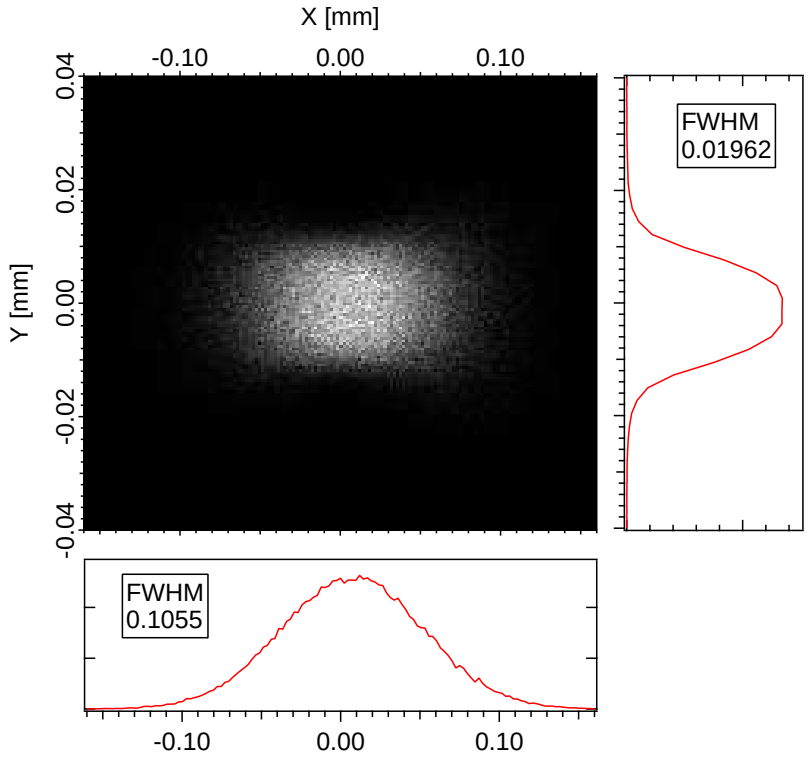

Figure 4: Spot pattern and beam intensity profiles at the sample plane at 17 eV (600 l/mm grating, c=2.25). The vertical exit slit opening was 50 μm while there was no limitation horizontally. FWHM values for the width and height show 106 μm and 20 μm, respectively. This image was obtained by simulating the solid state branch.

that would have required larger optical elements, not an economical solution for this beamline. The spot pattern at 17 eV photon energy is presented in Fig. 4 together with the horizontal and vertical beam profiles. Here the bow-tie shape is negligible and the profiles clearly show that most intensity is in the center, not in the wings.

5. Experimental stations

5.1. Gas phase end station

The beamline will have an end station for gas phase targets and samples whose vapor pressures are not suitable for UHV conditions. The gas phase branch line will therefore be equipped with a differential pumping section, similar to ones presented in Refs. [22, 23, 24, 25] and consisting of three stages: a 300 l/s turbo molecular pump, a line-of-sight differential ion pump from XIA and a 75 l/s ion pump. This allows a windowless pressure difference up to five orders of magnitude and an efficient removal of particles traveling along the photon beam, thus effectively protecting the refocusing mirror from contamination - a crucial requirement for gas-phase experiments.

Figure 5 shows a top view drawing of the gas phase end station. The vacuum system of this end station will contain two stages, and two measurement planes perpendicular to the beam direction. Each measurement plane can be set at the focal plane by moving the whole setup on rails along the photon beam. If the upstream stage is used for experiments, a vacuum tube with a capillary inside will be inserted between the experimental chamber and the differential pumping section. In the upstream chamber, the main instrument will be a Scienta R4000 electron spectrometer, equipped with a fast position-sensitive detector for photoelectron/photo-ion coincidence measurements (PEPICO). The instrument can also be used alone for high-resolution electron spectroscopy or in combination with detectors for other particles. In particular, a momentum-imaging multi-hit capable ion Time-of-Flight (TOF) spectrometer has been designed for this purpose. The control of the electron spectrometer and spectrum acquisition is executed by custom-made software and the ion and coincident electron-ion acquisition is performed using the CoboldPC software.

The downstream chamber of the gas phase end station will mostly be dedicated to photoluminescence experiments of solids. The lowest usable photon energy of the FinEstBeaMS beamline has actually been chosen considering the needs of photoluminescence studies. Excitations in the UV and VUV spectral

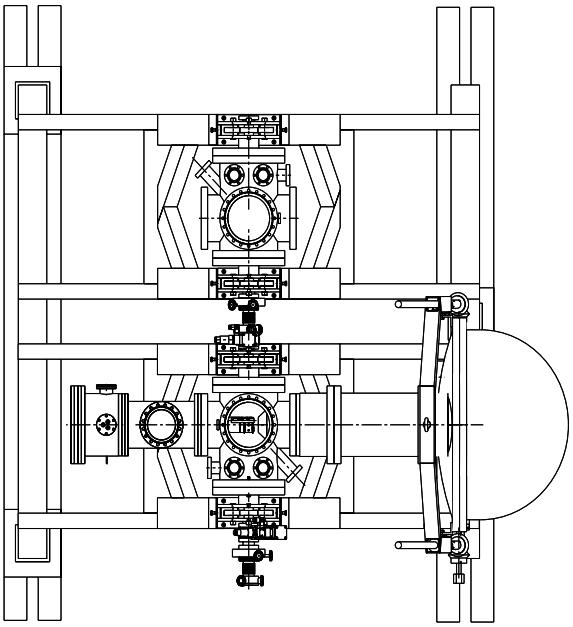

Figure 5: **Top view of the gas phase end station. The downstream vacuum chamber (below) hosts the photoelectron/photoion coincidence setup, which consists of the hemispherical Scienta R4000 electron analyzer and ion TOF spectrometer. Different instruments can be connected to the upstream vacuum chamber (above). The downstream chamber can be rotated in the plane perpendicular to the photon propagation direction. The two chambers can be moved together on rails along the photon beam to allow any of them to be placed at the focal plane.**

ranges are especially important for photoluminescence experiments because they allow one to examine all types of transitions in any solids having a band gap larger than 4 eV, i.e., wide band gap semiconductors and all insulators. For example, following low energy transitions could attract interest among users: transitions into the fundamental absorption edge of solids, any types of excitonic transitions, f-f and f-d transitions in rare-earth elements, and energy transfer processes from impurity atoms to the surrounding lattice. Furthermore, the analysis of luminescence spectra will greatly benefit from the possibility to focus exciting radiation in a tiny spot on solid samples. Luminescence experiments in high-pressure cells or in combination with high magnetic fields will also become feasible with highly focused synchrotron radiation. The photoluminescence setup will be equipped with a liquid helium closed cycle cryosystem, monochromators and detectors covering infrared, visible and ultraviolet spectral ranges. It will be used for any type of luminescence spectroscopy: steady-state and time-resolved emission and excitation spectroscopy as well as their temperature dependencies under ultraviolet and especially vacuum ultraviolet excitations. Also imaging measurements are foreseen.

The photoluminescence chamber can also be replaced by another chamber which can be used to mount various user instruments, for instance a magnetic-bottle-type electron TOF spectrometer. The latter will require both single-bunch operation of the storage ring and a beam chopper [26], hence it will not be available at the beginning of the operation of the MAX IV 1.5 GeV ring.

The end station is designed to accommodate various sample preparation systems that will be provided by both the FinEstBeaMS consortium and external users. In the first stage, gas inlet systems and solid target vaporization setups will be used.

5.2. Solid state end station

The solid state endstation will be a multipurpose spectroscopy end station that will provide versatile possibilities for the preparation and spectroscopic investigation of solid state materials via surface sensi-

tive experimental techniques. The end station will feature three vacuum chambers: an electron spectroscopy chamber (analysis chamber), a preparation chamber and a load-lock sample/sample storage chamber. The chambers will be fixed in geometry. All the chambers can be isolated and evacuated independently. The geometry of analysis and preparation chambers will be spherical and they will be in a vertical arrangement: the preparation chamber will sit on top of the analysis chamber. This is to optimize the main manipulator properties (mostly flow of cryogenic liquids, stability and precision) but also to minimize the footprint of the end station as the space for this end station will be restricted in the horizontal plane.

The analysis chamber will be designed for photoelectron spectroscopy (PES) and X-ray absorption spectroscopy (XAS). **The main instrument is a hemispherical electron energy analyser (PHOIBOS 150 2D-DLD from Specs), which is equipped with a delay line detector. The analyser will be mounted in a fixed port at a magic angle with respect to the photon beam and sample. It will have the focus at the sample, located at the center of the chamber. X-ray absorption spectra can be measured by collecting the drain current from the sample (total electron yield) or by recording Auger electrons with the electron energy analyser (Auger electron yield).** The chamber will be shielded against magnetic fields. The base pressure of the analysis chamber will be in the 10^{-10} mbar range. The chamber will be initially evacuated by a turbo pump (250-300 l/s), but the base pressure will be maintained by an ion pump (300 l/s). The ion pump will be isolated from the chamber by a gate valve.

The preparation chamber will be used for sample treatment processes such as Ar ion sputtering, physical vapor deposition (PVD), gas exposures and heat treatments. It will also facilitate sample transfer to and from the load-lock chamber. There will be a LEED/AES (low-energy electron diffraction / Auger-electron spectroscopy) system for structural and chemical composition analysis whenever there is no beam available. The base pressure of the preparation chamber will be $1{\cdot}10^{-9}$ mbar or better. The chamber will be initially evacuated

by a turbo pump, but the base pressure will be maintained by an ion pump (150 l/s). There will be a gate valve between the ion pump and the chamber since the ion pump must be isolated during high gas loads and especially during Ar ion sputtering.

The load-lock chamber will be adjunct to the preparation chamber. It will feature a sample transfer rod that enables sample transfer to and from the preparation chamber, a sample holder carousel for storing samples in vacuum, and a port for MAX IV vacuum suitcase. The base pressure of the load-lock chamber will be $1 \cdot 10^{-9}$ mbar or better. Samples will be inserted either through a DN63CF flange or via vacuum suitcase attached to the same port with an adapter. No Viton sealed quick access doors will be used in order to optimize the base pressure and minimize bake-out risks or catastrophic leaks due to bad sealing. The load-lock chamber will be pumped by a second turbo pump (100-200 l/s) for fast cycling.

6. Conclusions

The FinEstBeaMS beamline will receive radiation from an elliptically polarizing undulator in the photon energy range of 4.3-1000 eV. Even higher photon energies will be usable when the insertion device will be operated as a wiggler. The plane grating monochromator working with collimated light will achieve a resolving power of 5000-10000 in the whole operation range. This design takes advantage of recent development in grating manufacturing: low photon energies will be covered by using an extremely sparsely ruled grating instead of a NIM-like optical scheme. **A single ellipsoidal mirror will refocus radiation in each branch line. It will fulfill the requirement of the spot size, about 100 μm x 100 μm, and provide a horizontal beam at experimental end stations.** The simulations show that the considerable heat load can be handled with an efficient cooling scheme. The two branch lines will provide versatile settings for gas phase and solid state spectroscopies.

Acknowledgments

Main funding for the FinEstBeaMS beamline has been obtained from the European Union through the European Regional Development Fund (project "Estonian beamline to MAX-IV synchrotron", granted to the University of Tartu) and from the Academy of Finland through the Finnish Research Infrastructure funding projects. The authors also acknowledge the funding contributions of the University of Oulu, University of Turku, Tampere University of Technology, the Estonian Research Council (IUT2-25), as well as the Estonian Centre of Excellence in Research "Advanced materials and high-technology devices for sustainable energetics, sensorics and nanoelectronics" TK141 (2014-2020.4.01.15-0011). The authors thank the MAX IV Laboratory for financial and infrastructural support as well as for assistance during the construction of the FinEstBeaMS beamline. **They are grateful to Frank Siewert from Helmholtz-Zentrum Berlin for consultation and controlling the quality of the optical components of the FinEstBeaMS beamline.**

References

[1] `http://www.synchrotron-soleil.fr/Recherche/LignesLumiere/PLEIADES`

[2] R. Follath, F. Senf, Nucl. Instrum. Methods Phys. Res. A 390 (1997) 388.

[3] R. Follath, J.S. Schmidt, AIP Conf. Proc. 705 (2004) 631.

[4] U. Flechsig, L. Patthey, C. Quitmann, Nucl. Instrum. Methods Phys. Res. A 467-468 (2001) 479.

[5] S. Sasaki, K. Kakuno, T. Takada, T. Shimada, K. Yanagida, Y. Miyahara, Nucl. Instrum. Methods Phys. Res. A 331 (1993) 763.

[6] **E. Wallén, I. Blomqvist, J. Bahrdt, F.-J. Boegermann, Proceedings of IPAC2014, Dresden, Germany; TUPRO103, pages**

1286-1288. http://accelconf.web.cern.ch/AccelConf/IPAC2014/papers/tupro103.pdf

[7] T. Tanaka, H. Kitamura, J. Synchrotron Rad. 8 (2001) 1221.

[8] The Center for X-ray Optics, http://www.http://henke.lbl.gov/optical_constants/filter2.html

[9] S. Urpelainen, C. Såthe, W. Grizolli, M. Agåker, A.R. Head, M. Andersson, S.-W. Huang, B.N. Jensen, E. Wallén, H.Tarawneh, R. Sankari, R. Nyholm, M. Lindberg, P. Sjöblom, N. Johansson, B.N. Reinecke, M.A. Arman, L.R. Merte, J. Knudsen, J. Schnadt, J.N. Andersen, F. Hennies, J. Synchrotron Rad. 24 (2017) 344.

[10] R. Reininger, SRCalc, 2001-2009.

[11] COMSOL Multiphysics and Modeling v.3.5, www.comsol.com.

[12] F. Schäfers in: Springer Series in Modern Optical Sciences: Modern Developments in X- Ray and Neutron Optics, eds. A. Erko, M. Idir, Th. Krist, A.G. Michette, Springer Berlin/Heidelberg, 137 (2008) 9.

[13] R. Follath, G. Reichardt, O. Schwarzkopf, C. Jung, F. Senf, M. Weiss, BESSY Jahresbericht 1998 (1998) p. 470.

[14] P. Elleaume in: Undulators, Wigglers and Their Applications, eds. H. Onuki, P. Elleaume, Taylor & Francis, (2003) p. 69.

[15] W.B. Peatman, Gratings, Mirrors and Slits: Beamline Design for Soft-X-ray Synchrotron Radiation Sources, Gordon and Breach Science Publishers, Amsterdam (1997).

[16] O. Chubar, P. Elleaume, J. Chavanne, J. Synchrotron Rad. 5 (1998) 481.

[17] F. Schäfers, M. Krumrey, BESSY TB Nr. 201/96.

[18] R. Follath, private communication.

[19] V.N. Strocov, T. Schmitt, U. Flechsig, T. Schmidt, A. Imhof, Q. Chen, J. Raabe, R. Betemps, D. Zimoch, J. Krempasky, X. Wang, M. Grioni, A. Piazzalunga, L. Patthey, J. Synchrotron Rad. 17 (2010) 631.

[20] R. Follath, F. Senf, W. Gudat, J. Synchrotron Rad. 5 (1998) 769.

[21] M. Howells in New Directions in Research with Third-Generation Soft X-Ray Synchrotron Radiation Sources, Eds. A.S. Schlachter, F.J. Wuilleumier, Springer (1994).

[22] S. Aksela, A. Kivimäki, A. Naves de Brito, O.-P. Sairanen, S. Svensson, J. Väyrynen, Rev. Sci. Instrum. 65 (1994) 831.

[23] M. Bässler, A. Ausmees, M. Jurvansuu, R. Feifel, J.-O. Forsell, P. de Tarso Fonseca, A. Kivimäki, S. Sundin, S.L. Sorensen, R. Nyholm, O. Björneholm, S. Aksela, S. Svensson, Nucl. Instr. Meth. Phys. Res. A 469 (2001) 382.

[24] S. Urpelainen, M. Huttula, M. T. Balasubramanian, R. Sankari, P. Kovala, E. Kukk, E. Nõmmiste, S. Aksela, R. Nyholm, H. Aksela, AIP Conf. Proc. 1234 (2010) 411.

[25] J. Schnadt, J. Knudsen, J. Andersen, H. Siegbahn, A. Pietzsch, F. Hennies, N. Johansson, N. Mårtensson, G. Öhrwall, S. Bahr, S. Mähl, O. Schaff, J. Synchrotron Rad. 19 (2012) 701.

[26] D.F. Förster, B. Lindenau, M. Leyendecker, F. Janssen, C. Winkler, F.O. Schumann, J. Kirschner, A. Föhlisch, Opt. Lett. 40 (2015) 2265.

LaTeX Source Files

Click here to download LaTeX Source Files: BLpaperFINEST20170323 .zip